First-Principles Study on Stability and Electronic Structures of Pt-Rh Bimetallic Nanoparticles

AUTHOR(S):

Yuge, Koretaka; Ichikawa, Takayuki; Kawai, Jun

Materials Transactions, Vol. 51, No. 2 (2010) pp. 321 to 324

First-Principles Study on Stability and Electronic Structures of Pt-Rh Bimetallic Nanoparticles

Koretaka Yuge, Takayuki Ichikawa* and Jun Kawai

Department of Materials Science and Engineering, Kyoto University, Kyoto 606-8501, Japan

Energetic stability and electronic structures of Pt atoms in Pt-Rh nanoparticle is investigated by first-principles calculation. Pt atom energetically prefer surface sites (vertex, edge, and (100)) rather than subsurface and core site, which is attributed to lower Pt surface energy compared with Rh. Vertex of nanoparticle is the most favorable site for Pt atom, which has lowest coordination numbers. Band center of *d*-state electronic contribution for Pt atom measured from the Fermi energy exhibit negative dependence with respect to Pt coordination number. This can be attributed to positive dependence of second-order moment of density of states for the Pt *d*-band on the coordination number. Pt segregation to the surface is expected due mainly to contribution from Pt on-site segregation energy compared with weak ordering tendency of Pt-Rh unlike-atom pairs. [doi:10.2320/matertrans.M2009295]

(Received November 4, 2009; Accepted November 6, 2009; Published January 25, 2010)

Keywords: *first-principles, platinum, rhodium, alloy, nanoparticle, phase stability, electronic structure*

1. Introduction

Metal nanoparticles have been actively investigated so far for wide range of physical as well as chemical applications, since they are expected to show different properties from bulk due to finite-size effects and high surface-to-volume ratio.[1–5] In recent years, bimetallic nanoparticles are extensively studied and synthesized since alloying other elements can enhance catalytic properties. Theoretical study based on density functional theory (DFT) on bimetallic nanoparticles have been actively performed for such as Fe- and Pt-based alloys in order to investigate thermodynamically stable ordered structures and catalytic properties.[6–8] Pt-Rh nanoparticle is one of the most well-investigated system by experiments because of its enhanced catalytic property. The Pt-Rh nanoparticle are synthesized by variety of experiments including polyol synthesis method for clusters stabilized by ethylene glycol and OH^-, NaY-supported clusters using ion-exchange method, colloid synthesis in polymer solutions using borohydride-reduction, and pulsed laser ablation.[1,9–15] Since the catalytic property should significantly depend on its atomic arrangements, size, and composition, their structure have been carefully studied using such as Transmission Electron Microscope (TEM), Extended X-ray Absorption FineStructure (EXAFS), dispersive X-ray (EDX) analysis, and X-ray photoelectron spectroscopy (XPS). The synthesized particle typically has diameter with 1–4 nm and its atomic arrangements or preferably segregated species depends on sample preparation condition or method. Compared to constituent metal nanoparticle, the Pt-Rh nanoparticles can show higher catalytic properties for such as NO_x reduction, CO chemisorption, and hydrogenation.[15,16]

For Pt-Rh bulk surfaces, several first-principles investigation and experiments address the atomic structure and its related catalytic properties in order to design suitable alloy surface with high catalytic properties. Due to lower surface energy of Pt, small mixing enthalpy, and small difference in sublimation enthalpy, Pt atoms segregate to the topmost layer and depletion at the second layer, which are confirmed by both previous experimental[17–23] and theoretical[24–29] investigations. Recent first-principles-based investigation by the authors elucidate that Pt-Rh stable surface significantly destabilize CO adsorption with respect to hydrogen, which indicates the Pt-Rh surface to be potential candidate for electrode in polymer electrolyte fuel cells (PEFC): The destabilization is reasonably attributed to the *d*-state electronic contribution of top-layer Pt atoms, particularly to the *d*-band center measured from the Fermi energy. DFT-based studies on Pt and Rh nanoparticles have also been carried out to understand stable atomic configurations:[30–36] Up to now, nanoparticles consisting of ~ 300 atoms are extensively studied, and a number of stable or metastable structures including icosahedron, octahedron, cuboctahedron, biplanar, and lower-symmetry shapes are proposed, where their relative stability is still under discussion. Particularly, icosahedral and cubohedral Pt and Rh nanoparticles have been considered interesting since they are Platonic and Archimedean solids in uniform polyhedra, and they are linked to each other by Mackay transformation with small energy difference.[31]

In contrast to such stimulating experimental as well as theoretical investigations for Pt, Rh and Pt-Rh nanoparticles and bulk surfaces, theoretical studies on the Pt-Rh nanoparticle is somehow confined to segregation profile predicted by empirical method including pair-bond energy model[37] and free energy concentration expansion:[38] These studies predict Pt atoms energetically prefer to segregating to the surface rather than subsurfaces. With these considerations, further theoretical assessment for electronic structure and catalytic properties of the Pt-Rh nanoparticles based on first-principles calculation is highly desirable in order to design suitable alloy nanoparticles. In the present study, we concentrate on study of Pt-Rh nanoparticle consisting of 55 atoms with cuboctahedron shape where the 55-atom nanoparticle is considered interesting due to its intermediate size between finite molecules and fully metallic systems[34] and cuboctahedron nanoparticle has been studied based on semiempirical model for segregation in Pt-Rh system, and

*Graduate Student, Kyoto University

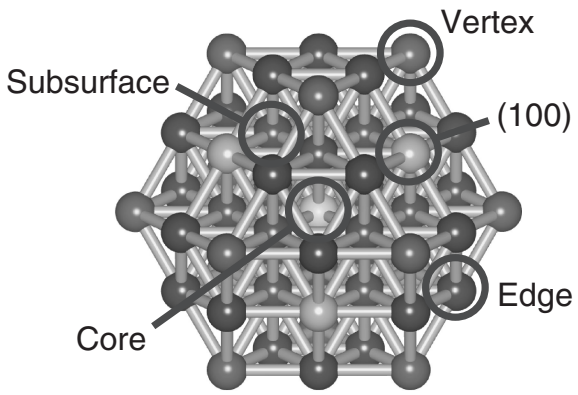

Fig. 1 Schematic illustration of Pt-Rh nanoparticle used in the present calculation. Symmetry-nonequivalent sites are distinguished by color.

is also synthesized for 55 Pt atoms.[38–40] We perform first-principles calculation on Pt_1Rh_{54} and Pt_2Rh_{53} nanoparticles: Energetically preferred single site of Pt atom, Pt electronic structure and ordering tendency for the Pt-Rh nanoparticles are discussed.

2. Methodology

In order to investigate energetic stability and electronic structure of Pt atom for Pt-Rh nanoparticle, we construct cuboctahedron consisting of 55-atoms described above. Since 42 among the 55 atoms are located at the surface, significant size-effects for nanoparticle can be expected. Figure 1 shows schematic illustration of the used particle. There are five symmetry-nonequivalent sites: vertex, edge, (100), subsurface, and core. For Pt_1Rh_{54} nanoparticle, we have five types of Pt-Rh nanoparticle where single Pt atom occupies one of the five nonequivalent site, and other 54 sites are occupied by Rh atoms. For Pt_2Rh_{53} nanoparticle, we replace two Pt atoms at all the pair combination of the five symmetry-nonequivalent sites in minimum distance, as shown in Fig. 2: There are 14 atomic configurations.

We perform the first-principles calculations using DFT code, Vienna *Ab-initio* Simulation Package (VASP).[41–43] The all-electron Kohn-Sham equations were solved by employing the projector augmented-wave (PAW) method.[44] The exchange-correlation functional was described by generalized gradient approximation (GGA) of Perdew-Wang91 form.[45] Plane-wave cutoff energy was set to 576.7×10^{-19} J (360 eV) throughout the calculation. The numerical error was estimated to be of the order of 1.6×10^{-22} J/atom (1 meV/atom) by cutoff convergence tests. To deal with the possible convergence problems for metals, Methfessel-Paxton scheme[46] was used with a smearing parameter σ of 0.128×10^{-19} J (0.08 eV). k-points sampling are performed on the basis of the Monkhorst-Pack scheme[47] with $1 \times 1 \times 1$ grids. We put 55-atom nanoparticle in cubic cell with each side of 2 nm, which is confirmed to be sufficient in terms of cell-size dependence of total energy. Geometry optimization under the condition of fixed cell size and shape is performed until residual forces on each atoms become less than 4.81×10^{-20} J/nm (0.03 eV/Å).

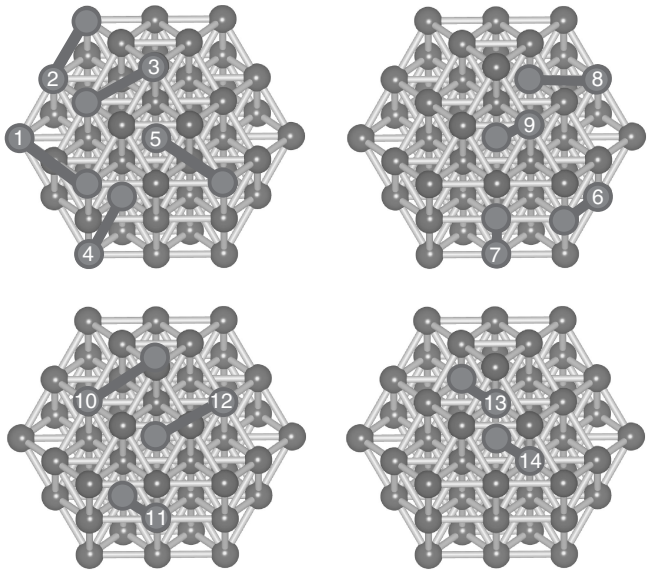

Fig. 2 Schematic illustration of positions of two Pt atoms in Pt_2Rh_{53} nanoparticles, which are illustrated by dark shperes connected with dark bold lines.

Table 1 Calculated relative total energy of Pt_1Rh_{54} nanoparticle E_{rel}, coordination number for Pt atom Z, and d-band center of Pt atoms, ϵ_d.

Pt position	$E_{on-site}$/1.6e-19 J (eV)	Z	ϵ_d/1.6e-19 J (eV)
vertex	−0.55	5	−2.07
edge	−0.49	7	−2.14
(100)	−0.39	8	−2.22
subsurface	0.07	12	−3.26
core	0	12	−3.35

3. Results and Discussion

We first investigate energetics of the modeled Pt_1Rh_{54} nanoparticles in order to see energetically favorable single Pt site. Table 1 summarizes total energy of the nanoparticles measured from that of nanoparticle with Pt atom at core site (we call on-site energy, $E_{on-site}$ hereinafter), coordination number of Pt atom (Z), and d-band center of Pt atom measured from the Fermi energy (ϵ_d) for the five modeled nanoparticles. For bulk, Pt segregates to surface due to lower Pt surface energy compared with Rh and Rh segregates to 2nd layer due to positive Pt segregation energy.[27–29] From Table 1, similar tendency can be seen: For three sites at surface (vertex, edge, and (100)), on-site energies exhibit negative sign, while that for subsurface exhibit positive sign. Therefore, when we assume weak mixing contribution to the total free energy, which holds for bulk Pt-Rh alloy, Pt prefers sites at the surface. This is consistent with early theoretical prediction based on empirical methods.[37,38] At the surface, on-site energy increase in negative sign when coordination number of Z decreases. This can be attributed to the fact that Pt segregates to a site with lower coordination number in order to decrease surface energy of the nanoparticle. This is because since surface energy increase for lower coordination surface by a factor of $\sqrt{Z}$ within effective medium approximation up to second-order

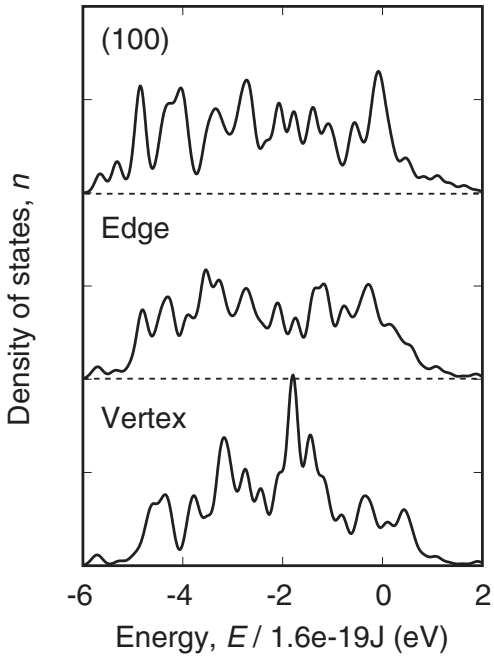

Fig. 3 Calculated density of states from d-state contribution measured from Fermi energy for the three surface sites of vertex, edge, and (100).

moment, negative energy gain by Pt-atom segregation should be more enhanced for sites with lower coordination number.

Next, we investigate the electronic structure of Pt atom in the nanoparticle. We show in Fig. 3 the calculated electronic density of states from d-state contribution measured from Fermi energy for the three surface sites. From Fig. 3, no significant difference can be found for the three surface sites. Corresponding d-band center, ϵ_d, are described in Table 1. ϵ_d ranges from -3.56 to -3.32×10^{-19} J (-2.22 to -2.07 eV), which are larger in negative sign than $\epsilon_d = -3.24 \times 10^{-19}$ J (-2.02 eV) for $Pt_{25}Rh_{75}$ ground-state bulk alloy surface.[29] Another important point in Table 1 is that ϵ_d move down from Fermi energy with increase in coordination number, Z. Particularly, subsurface and core sites with $Z = 12$ have significantly lower ϵ_d of around 5.28×10^{-19} J (-3.3 eV). These can be attributed to the fact that: When coordination number for Pt atom increase, second-order moment of Pt d-band should naturally increase due to increase in hybridization with nearest-neighbor Rh atoms. Since Pt has more than half-filled $5d$ shells, downshift of the d-band center should be more enhanced for larger coordination numbers to conserve the charges. In order to intuitively see this, we show in Fig. 4 the second order moment of Pt d-band with respect to the d-band center as a function of coordination number for the Pt atom. We can clearly see from Fig. 4 that almost linear dependence of the second-order moment on coordination number is certainly satisfied, which should lead to downshift of the Pt d-band in terms of coordination number described above. The downshift of Pt d-band center can also be found for Pt-Rh alloy surface by our previous work, which causes destabilization of CO adsorption with respect to H adsorption. This indicates that Pt-Rh nanoparticle can be potential candidate for electrode catalysis in polymer electrolyte fuel cells (PEFC).

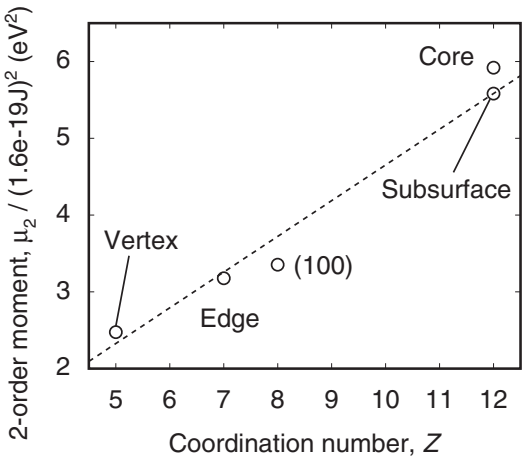

Fig. 4 Second order moment of Pt d-band with respect to the d-band center, as a function of coordination number for the Pt atom.

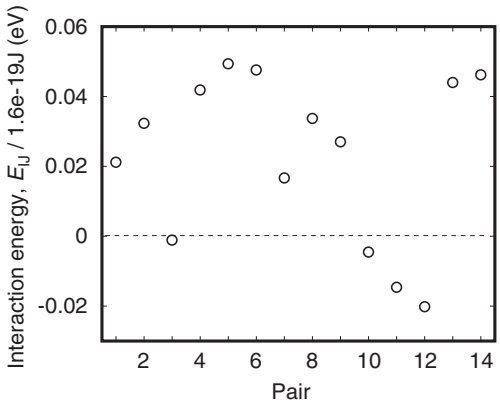

Fig. 5 Calculated Pt-Pt interaction energy defined by eq. (1) for pairs shown in Fig. 2.

Finally, we investigate energetics of ordered Pt_2Rh_{53} nanoparticles to see ordering contribution to stability for Pt-Rh nanoparticle. In order to understand energetic preference of Pt atoms, we introduce following Pt pair interaction energy given by

$$E_{\mathrm{I-J}} = E_{\mathrm{I-J}}^{\mathrm{Pt_2Rh_{53}}} - (E_{\mathrm{I}}^{\mathrm{Pt_1Rh_{54}}} + E_{\mathrm{J}}^{\mathrm{Pt_1Rh_{54}}} - E^{\mathrm{Rh_{55}}}), \qquad (1)$$

where $E_{\mathrm{I-J}}^{\mathrm{Pt_2Rh_{53}}}$, $E_{\mathrm{P}}^{\mathrm{Pt_1Rh_{54}}}$ and $E^{\mathrm{Rh_{55}}}$ denote total energy of Pt_2Rh_{53} nanoparticle with two Pt atoms at site I and J, that of Pt_1Rh_{54} with single Pt atom at site P, and that of Rh_{55} nanoparticle, respectively. Thus $E_{\mathrm{I-J}}$ represents relative energy of Pt pairs at I and J sites with respect to two Pt atoms isolately located at I and J sites without interaction. Therefore, $E_{\mathrm{I-J}} < 0$ indicates preference of Pt pair at I and J site, and $E_{\mathrm{I-J}} > 0$ disfavor the Pt-Pt pair. Figure 5 shows the interaction energy for Pt pairs shown in Fig. 2. Most of the interaction energies (10 of 14) exhibit positive sign with larger value compared with those in negative sign, indicating that Pt pairs are energetically unfavored and Pt-Rh unlike-atom pairs are favored in the Pt-Rh nanoparticle, which is a similar ordering tendency of bulk Pt-Rh alloy.[29] Another important point in Fig. 5 is that $E_{\mathrm{I-J}}$s are in one-order smaller than Pt on-site energies described in Table 1. This indicates that Pt on-site energy should be dominant and ordering

tendency is predominant contributions to surface segregation in the Pt-Rh nanoparticle. Therefore, Pt-Rh nanoparticle is expected to show similar segregation behavior to Pt-Rh bulk surface, where strong Pt segregation is mainly attributed to Pt on-site energy contribution.[29)]

4. Conclusions

We perform first-principles calculations in order to examine energetic stability and electronic structures of Pt atoms in Pt-Rh nanoparticle. Single Pt atom energetically prefer surface sites of vertex, edge, and (100) rather than subsurface and core sites. This can be attributed to the fact that Pt tend to prefer sites with lower coordination number so that surface energy of the nanoparticle decreases, which have also been seen in Pt-Rh bulk alloy surface. *d*-band center for Pt atom exhibit negative dependence with respect to Pt coordination number. This can be attributed to increase in second-order moment of the Pt *d*-band for increase in the coordination number. Ordering tendency for Pt-Rh nanoparticle is also investigated. Pt-Rh unlike-atom pairs are energetically preferred, which is a similar tendency in Pt-Rh bulk alloy. Pt segregation to the surface of Pt-Rh nanoparticle is expected due to the dominant contribution of Pt on-site energy compared with weak ordering tendency.

Acknowledgements

This research was supported by Grant-in-Aid for Young Scientists Start-up (20860048).

REFERENCES

1) N. Toshima and T. Yonezawa: New J. Chem. **1** (1998) 1179–1201.
2) M. Valden, X. Lai and D. W. Goodman: Science **281** (1998) 1647–1650.
3) J. Meier, K. A. Friedrich and U. Stimming: Faraday Discuss. **121** (2002) 365–372.
4) N. Lopez and J. K. Norskov: J. Am. Chem. Soc. **124** (2002) 11262–11263.
5) F. Maillard, M. Eikerling, O. V. Cherstiouk, S. Schreier, E. Savinova and U. Stimming: Faraday Discuss. **125** (2004) 357–377.
6) Y. Wang, G. M. Stocks, A. Rusanu, D. M. C. Nicholson, M. Eisenbach, Q. Zhang and J. P. Liu: IEEE Trans. Mag. **43** (2007) 3103–3105.
7) A. A. Franco, S. Passot, P. Fugier, C. Anglade, E. Billy, L. Guétaz, N. Guillet, E. De Vito and S. Mailley: J. Electrochem. Soc. **156** (2009) B410–424.
8) M. E. Gruner and A. Dannenberg: J. Mag. Mag. Mater. **321** (2009) 861–864.
9) N. Savastenko, H. R. Volpp, O. Gerlach and W. Strehlau: J. Nanopart Res. **10** (2008) 277–287.
10) Y. Wang, J. Zhang, X. Wang, J. Ren, B. Zuo and Y. Tang: Topics Catal. **35** (2005) 35–41.
11) M. Harada, K. Asakura and N. Toshima: J. Phys. Chem. **98** (1994) 2653–2662.
12) T. Hashimoto, K. Saijo, M. Harada and N. Toshima: J. Chem. Phys. **109** (1998) 5627–5638.
13) M. Harada and H. Einaga: J. Colloid. Int. Sci. **308** (2007) 568–572.
14) E. Cimini and R. Prins: J. Phys. Chem. B **101** (1997) 5285–5293.
15) K. Siepen, H. Bönnemann, W. Brijoux, J. Rothe and J. Hormes: Appl. Organometal. Chem. **14** (2000) 549–556.
16) C. E. Lyman, R. E. Lakis and H. G. Stenger: Ultramicroscopy **58** (1995) 25–34.
17) F. C. M. J. M. van Delft and B. E. Nieuwenhuys: Surf. Sci. **162** (1985) 538–543.
18) A. D. van Langeveld and J. W. Niementsverdriet: Surf. Sci. **178** (1986) 880–887.
19) D. M. Ren and T. T. Tsong: Surf. Sci. **184** (1987) L439–L444.
20) P. Verga and M. Schmid: Appl. Surf. Sci. **141** (1999) 287–293.
21) E. Platzgummer, M. Sporn, R. Koller, S. Forsthuber, M. Schmid, W. Hofer and P. Varga: Surf. Sci. **419** (1999) 236–248.
22) E. L. D. Hebenstreit, W. Hebenstreit, M. Schmid and P. Varga: Surf. Sci. **441** (1999) 441–453.
23) D. Brown, P. D. Quinn, D. P. Woodruff, T. C. Q. Noakes and P. Bailey: Surf. Sci. **497** (2002) 1–12.
24) B. Legrand and G. Tréglia: Surf. Sci. **236** (1990) 398–408.
25) J. Florencio, D. M. Ren and T. T. Tsong: Surf. Sci. **245** (1996) L29–L33.
26) L. Z. Mezey and W. Hofer: Surf. Sci. **402–404** (1998) 845–850.
27) A. V. Ruban and H. L. Skriver: Comput. Mater. Sci. **15** (1999) 119–143.
28) S. Müller, M. Stöhr and O. Wieckhorst: Appl. Phys. A **82** (2006) 415–419.
29) K. Yuge, A. Seko, A. Kuwabara, F. Oba and I. Tanaka: Phys. Rev. B **74** (2006) art. no. 174202 1–13.
30) S. K. Nayak, S. E. Weber, P. Jena, K. Wildberger, R. Zeller, P. H. Dederichs, V. S. Stepanyuk and W. Hergert: Phys. Rev. B **56** (1997) 8849–8854.
31) C. Barreteau, M. C. Desjonquëres and D. Spanjaard: Eur. Phys. J. D **11** (2000) 395–402.
32) L. Wang and Q. Ge: Chem. Phys. Lett. **366** (2002) 368–376.
33) V. Kumar and Y. Kawazoe: Eur. Phys. J. D **24** (2003) 81–84.
34) E. Aprà and A. Fortunelli: J. Phys. Chem. **107** (2003) 2934–2942.
35) L.-L. Wang and D. D. Johnson: Phys. Rev. B **75** (2007) art. no. 235405 1–10.
36) V. Kumar and Y. Kawazoe: Phys. Rev. B **77** (2008) art. no. 205418 1–10.
37) A. de Sarkar and B. C. Khanra: Chem. Phys. Lett. **353** (2002) 426–430.
38) R. Vardi, L. Rubinovich and M. Polak: Surf. Sci. **602** (2008) 1040–1044.
39) K. Kinoshita: J. Electrochem. Soc. **137** (1990) 845–848.
40) M. J. Yacaman, J. A. Ascencio, H. B. Lui and J. Gardea-Torresdey: J. Vac. Sci. Technol. B **19** (2001) 1091–1103.
41) G. Kresse and J. Hafner: Phys. Rev. B **47** (1993) R558–561.
42) G. Kresse and J. Furthmüller: Phys. Rev. B **54** (1996) 11169–11186.
43) G. Kresse and D. Joubert: Phys. Rev. B **59** (1999) 1758–1775.
44) P. E. Blöchl: Phys. Rev. B **50** (1994) 17953–17979.
45) J. P. Perdew and Y. Wang: Phys. Rev. B **45** (1992) 13244–13249.
46) M. Methfessel and A. T. Paxton: Phys. Rev. B **40** (1989) 3616–3621.
47) H. J. Monkhost and J. D. Pack: Phys. Rev. B **13** (1976) 5188–5192.